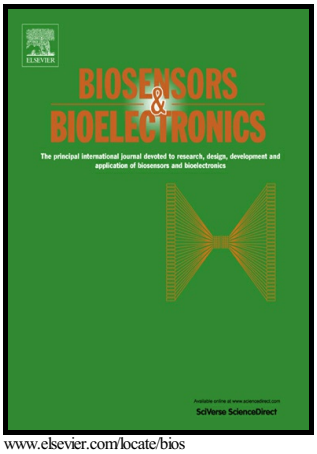

www.elsevier.com/locate/bios

Gold Dendrites Co-deposited with M13 Virus as a Biosensor Platform for Nitrite Ions

Yeji Seo, Shanmugam Manivannan, Inhak Kang, Seung-Wuk Lee, Kyuwon Kim

PII: S0956-5663(17)30122-7
DOI: http://dx.doi.org/10.1016/j.bios.2017.02.036
Reference: BIOS9570

To appear in: *Biosensors and Bioelectronic*

Received date: 19 December 2016
Revised date: 15 February 2017
Accepted date: 22 February 2017

Cite this article as: Yeji Seo, Shanmugam Manivannan, Inhak Kang, Seung-Wuk Lee and Kyuwon Kim, Gold Dendrites Co-deposited with M13 Virus as a Biosensor Platform for Nitrite Ions, *Biosensors and Bioelectronic* http://dx.doi.org/10.1016/j.bios.2017.02.036

Gold Dendrites Co-deposited with M13 Virus as a Biosensor Platform for Nitrite Ions

Yeji Seo [a,†], Shanmugam Manivannan [a,†], Inhak Kang[a], Seung-Wuk Lee[b] and Kyuwon Kim[a,*]

[a]Electrochemistry Laboratory for Sensors & Energy (ELSE)
Department of Chemistry, Incheon National University, Incheon 406-772, Republic of Korea.
[b]Department of Bioengineering, University of California, Berkeley, California 94720, USA
Incheon 406-772, Republic of Korea.
*E-mail: kyuwon_kim@inu.ac.kr
[†]Both authors contributed equally

Abstract:

We developed a biosensor for nitrite ion on an electrode surface modified with M13 viruses and gold nanostructures. Gold dendritic nanostructures (Au-DNs) are electrochemically co-deposited from 4E peptides engineered M13 virus ($M13_{4E}$) mixed electrolyte on to the ITO electrode. The $M13_{4E}$ could specifically nucleate Au precursor (Gold (III) chloride), which enable the efficient growth of dendritic nanostructures, whereas such dendritic structures were not obtained in the presence of wild-type and Y3E peptides engineered M13 viruses. The structural features of the Au-DNs and their interfacing mechanism with ITO electrode are characterized by SEM, EDX and XRD analyses. The growth of Au-DNs at ITO electrode has been monitored by time dependent SEM study. The $M13_{4E}$ induces the formation and plays a crucial role in shaping the dendritic morphology for Au. Biosensor electrode was constructed using Au-DNs modified electrode for nitrite ions and found improved sensitivity relative to the sensor electrode prepared from wild-type M13, Y3E peptides engineered M13 and without M13. Sensor electrode exhibited good selectivity toward target analyte from the possible interferences. Furthermore, 4E native peptides were used as additive to deposit Au nanostructures and it is compared with the structure and reactivity of the Au nanostructures prepared in the presence of $M13_{4E}$. Our novel biosensor fabrication can be extended to other metal and metal oxide nanostructures and its application might be useful to develop novel biosensor electrode for variety of biomolecules.

Keywords: Biosensor, Electrodeposition, Gold nanostructures, M13 virus, Nitrite ions

1. Introduction

Nitrite (NO_2^-) is an important inorganic pollutant to the environment and human health which is majorly originated from food, corrosion inhibitors and fertilizers.(Peteu et al. 2014) The crucial obstacle caused by NO_2^- is when at high concentration its interaction with amines to form carcinogenic nitrosamines, resulting in serious hazards to human and animal health.(Palanisamy et al. 2014; Radhakrishnan et al. 2014) In drinking water 3 mg/L is the maximum limit value of NO_2^- recommended by the World Health Organization.(Mehmeti et al. 2016) Fertilizers are the major NO_2^- source for polluting the water (sea, ground, lake, river and rain water). Hence, more precise estimation of NO_2^- is an important task for environmental and water sources safety. Among the variety of techniques (based on spectroscopy, chromatography and electrochemistry) available for the quantification of NO_2^-, electroanalytical methods based on modified electrodes attracts more attention due to its easy fabrication, handling and economic aspects.(Kim et al. 2016) Therefore, it is important to develop potential electrode materials for the oxidation of NO_2^- to fabricate highly selective sensors. Indium tin oxide (ITO)-coated glass is a widely used electrode material due to its large potential window and excellent optical transparency. It has been observed that, background current could be minimized by using ITO electrodes.(Hong et al. 2008; Shin et al. 2011) Also, ITO electrodes as a solid support can avoid the need for the complex and laborious cleaning steps required for other common solid electrodes.(Khan et al. 2013) To decrease the operating potential and to increase the sensitivity and selectivity usually electrodes are modified with the variety of metal and metal oxide nanostructures (NSs) (Bharath et al. 2015; Pham et al. 2014; Radhakrishnan et al. 2014; Teymourian et al. 2013) and biomolecules.(Peteu et al. 2014; Shervedani et al. 2016) In particular gold (Au) based electrocatalysts demonstrated excellent electrochemical responses towards the detection and determination of NO_2^- because it can facilitate a fast electron transfer between redox centers in small molecules and electrode surfaces, and be used as catalysts to increase the rate

of electrochemical reactions.(Rao et al. 2016; Shanmugam and Kim 2016; Shervedani et al. 2016; Yadav et al. 2016)

In recent years, the use of display technologies has developed as a commanding tool to screen peptides with recognition for the surface of metal and metal oxide NSs. Thereby biological molecules (DNA, peptides, proteins and viruses) have developed unique abilities to grow and assemble NSs with an impressive degree of control known as biomineralization.(Nam et al. 2006; Sun et al. 2014; Wu et al. 2012; Xu et al. 2015) These biological molecules are useful templates because of their molecularly precise shapes and the spatial organization that they communicate with NSs, as well as specific affinities for binding to the surfaces and nucleating and assembling NSs into functional assemblies with useful electrical and optical properties.(Avery et al. 2009; Ki et al. 2008; Mao et al. 2003; Mateu 2011) There have been reports on the assembly of NSs in solution and the directed immobilization of NSs on substrates using biological molecules-based recognition systems.(Stevens et al. 2004; Zin et al. 2005) In particular, the M13 virus (M13) has been extensively used for its ability to bind selectively to a variety of NSs. Its NSs-specific binding and nucleation capabilities are typically identified through a multistep biopanning process.(Qi et al. 2014) M13 is a bacterial virus that infects bacterial host cells and it is filamentous and has a cylindrical shape with a diameter of 6 nm and a length of 880 nm. Its genetically modifiable outer protein coat composed of 2,700 identical protein subunits. It encapsulates a single-strand genome that encodes five different capsid proteins (Figure 1).(Hemminga et al. 2010; Lee et al. 2006)

Recently, M13 has been found as the promising biotemplate for variety of metal and metal oxide NSs and used as an electrode material for sensor, energy and biomedical applications. Researchers mainly focusing on identifying and exploiting the binding peptides of M13 that are specific for certain material, and it could capable of nucleating and growing NSs along with its filamentous structure to obtain biotemplated nanowires. For instance, Lee and co-workers developed the Quantum dot-engineered M13 based sensor for TNT(Jin et al. 2013) and Belcher and co-workers

reported the metal alloy and iridium oxide nanostructured M13 templated nanowires for different applications.(Lee et al. 2010; Nam et al. 2012) Besides, so far to template metal NSs with M13, researchers are following solution-based biomineralization methods with the assistance of external reducing agents and they are often suffering from product stability, purification and handling for device fabrication. On the other hand, via electrodeposition size and shape can be easily tuned by altering experimental parameters (time, potential and electrolyte concentration) also no external reducing and stabilizing agents are required. Here, we show that electrostatic interactions between cationic Au metal precursors and the anionic carboxylate groups of the 4E peptides engineered M13 ($M13_{4E}$), followed by electrochemical co-deposition, can generate M13 templated dendritic NSs (DNs) without the need for structure directing surfactants. Biosensor electrode has been constructed for the sensitive and selective determination of NO_2^-.

2. Experimental Section

2.1. Materials and Methods

Gold (III) chloride hydrate ($HAuCl_4.3H_2O$), L-ascorbic acid (AA), Sodium nitrite and D-(+)-Glucose were received from Sigma-Aldrich. Native 4E peptides (4E Pep) were received from Anygen. All the chemicals were of analytical grade and were used as received. FESEM images were recorded with JEOL JSM-7800F instrument. XRD profiles were recorded using Smart Lab (Rigaku) instrument. Indium tin oxide (ITO, (dimension; 2×1 cm)) and its modified forms were used as working electrodes. Pt wire served as a counter electrode and Ag/AgCl (in 3 M NaCl solution) was used as a reference electrode. All the electrochemical experiments were conducted in a single compartment three electrode cell using an Ivium Technologies electrochemical work station. Nitrogen (N_2) was bubbled for 30 minutes prior to each experiment.

2.2a. Wild-type M13 ($M13_{wild}$) preparation

$M13_{wild}$ was grown and purified following standard biochemical protocols described in literature.(Korkmaz 2013; Smith and Petrenko 1997) Briefly, one colony of E. coli XL-1 blue was

grown in 3 ml of LB media to mid-log phase (E. coli XL-1 blue culture) and infected with 10 µL of $M13_{wild}$. The culture was incubated at 37°C with shaking for 12 h, and then centrifuged to remove E. coli. The $M13_{wild}$ was collected by PEG/NaCl (20% PEG and 2.5 mol/L NaCl) precipitation and reconstituted in Tris-bufferred saline (10 mM). The typical yield was ~ 20 mg of $M13_{wild}$ per litter. The final concentration was determined spectrophotometrically using an extinction coefficient of 3.84 cm^2/mg at 269 nm.(Sambrook and Russell 2001; Smith and Petrenko 1997)

2.2b. Y3E peptides engineered M13 ($M13_{Y3E}$) and $M13_{4E}$ preparation

Attachment of Au binding peptides at the major coat protein (Gene VIII) of M13 is reported previously.(Park et al. 2014) Briefly, three primers were designed to insert Y3E and 4E into the gene VIII protein: 5′-ATATATCTGCAGNKTAYGAAGAGGAANNKGATCCCGCAAAAGCGGCCTTTA ACTCCC-3′ (Y3E), 5′-ATATATCTGCAGNKGAAGAGGAAGAGCCCGCAAAAGCGGCCTTTAA CTCCC-3′ (4E), and 5′-GGAAGCTGCAGCGAAAGACAGCATCGGAACGAGG-3′ (linearization primer). To collect $M13_{Y3E}$ and $M13_{4E}$ phages, the inverse polymerase chain reaction (PCR) cloning method was performed using the above mentioned primers (the linearization primer with $M13_{Y3E}$ and $M13_{4E}$ primer). The PCR product was purified then the amplified plasmid, and phage plagues were verified by DNA sequencing. Furthermore, we have amplified the $M13_{Y3E}$ and $M13_{4E}$ phage for our experiments, and the methods were same to the $M13_{wild}$ as mentioned in 2.2a.(Sambrook and Russell 2001; Smith and Petrenko 1997) Figure 1 demonstrates the structural features of the different M13 used in this study.

2.3. Fabrication of modified electrodes

Au NSs were electrodeposited on ITO electrode from the electrolyte (mixture of 3 mM of $HAuCl_4.3H_2O$ and 0.005 mg/mL of $M13_{wild}$ or $M13_{Y3E}$ or $M13_{4E}$ or 4E Pep in 0.5 M H_2SO_4) by applying the potential of –0.2 V (Ag/AgCl) for 500 s by amperometric i-t curve technique. Fabricated electrodes was denoted as ITO/Au or ITO/Au_{wild} or ITO/Au_{Y3E} or ITO/Au_{4E} or ITO/Au-

4E Pep. After the experiment, the charge (Q) was integrated from 0 to 500 s and the same was used to estimate the specific mass (M) of Au using the eq 1.

$$M = Q \times MW / (n\ FA) \qquad (1)$$

where 'M' is specific mass after electrodeposition, 'Q' is charge consumed for electrodeposition, 'MW' is the molecular mass of Au, 'n' is number of electrons (3) transferred for electrodeposition, 'F' is Faraday constant and 'A' is geometrical area (0.44 cm^2) of the electrode ('O' ring). The mass of Au was used to normalize the current to obtain current density plots. The electrochemically active surface area (ECSA) was calculated from the charge consumed to form the Au oxide monolayer at the different modified electrodes using eq 2 (Trasatti and Petrii 1992) and was used to obtain the current density plots.

$$EASA = Q/Q^* \qquad (2)$$

where 'Q' is the charge required to form an oxide monolayer on the surfaces of Au NSs, which is obtained by measuring the charge (Q) associated with the Au oxide reduction peak as a function of upper potential limit and Q* is calibration factor with a value of 390 μC cm^{-2}. (Correia et al. 1997; Trasatti and Petrii 1992) The Q* is the standard value associated with the formation of oxide monolayer at polycrystalline Au surface.

2.4. Electrochemical studies

The NO_2^- electrocatalysis, sensing and selectivity studies at the modified electrodes were studied by recording the cyclic voltammograms (CVs) and Linear sweep voltammograms (LSVs). For the electrocatalytic measurements by CV, 1 mM of sodium nitrite was added to the 0.1 M PBS (pH 7.2) electrolyte and for sensing by LSV each 100 μM of sodium nitrite was added. The selectivity experiments toward NO_2^- were carried out with the 40 times higher concentrated commonly encountered metal cations, anions and biomolecules. All the experiments were carried out at the room temperature (25° C) with a potential window of 0 to 1.2 V.

3. Results and discussion

3.1. Surface characterization of the modified electrodes

The comprehensive information about the surface morphology and the consistency of the modified electrodes can be observed by scanning electron microscopy (SEM). The surface morphology of the ITO/Au, ITO/Au_{wild}, ITO/Au_{Y3E}, ITO/Au_{4E} electrodes were investigated by SEM (Figure 2). As can be seen in Figure 2(A and A1), flowerlike Au NSs were grown at the ITO surface in the absence of any of the M13. When M13 is mixed in the electrolyte, change in the morphology are clearly visible in Figure 2(B,C and D) when compared to ITO/Au electrode. Close view (Figure 2(B1 and C1) of the $M13_{wild}$ and $M13_{Y3E}$ applied Au NSs resembles with the popcorn-like structures. Furthermore, close view of these flower-like and popcorn-like Au NSs (Figure 2(A1, B1 and C1) did not show any preferential growth along a specific crystallographic direction. Whereas, Au DNs were clearly visible at the ITO/Au_{4E} electrode; SEM image (Figure 2D1) clearly shows the formation of Au-DNs. Presence of $M13_{4E}$ and its 4E peptides had a considerable effect on controlling shape(Kim et al. 2010; Zhang et al. 2014) and structure of Au-DNs. Figure S1 displays the SEM images at different magnifications and EDX analysis of ITO/Au_{4E} electrode. Based on the diffusion and nucleation limited aggregation models, growth of Au-DNs at ITO/Au_{4E} electrode is possibly controlled by diffusion and nucleation process in non-equilibrium reactions.(Xiao and Qi 2011) In the absence of M13 (Figure 2(A and A1)), deposited Au possessing densely packed flower-like NSs, suggesting the deposition rate was rapid and independent of crystallographic direction at the electrode surface.(Yue et al. 2011) In addition, to trace the nucleation and growth of Au-DNs at ITO/Au_{4E} electrode; SEM images were recorded at different deposition time and different $M13_{4E}$ concentration as shown in Figures 3 and S2, respectively. As can be seen at 5 and 10 s (Figure 3A and B) Au dendritic seeds were clearly formed. And at 20 s (Figure 3C) dendritic growth has started and branches are clearly visible. Interestingly after 20 s, secondary growth of Au-DNs has actually started. From 50 s onwards Au-DNs were clearly observed (Figure 3(D,E and F). On the other hand

while increasing the concentration of $M13_{4E}$ starting from 0.001 to 0.1 mg/mL, clear structural variation of DNs to flower-like NSs were observed (Figure S2). Furthermore, the trunk size and shape has shrinking while increasing the $M13_{4E}$ concentration and led to such flower-like NSs. Figure S3 displays the XRD patterns of the four different modified electrodes and in all the four electrodes the diffraction peaks appeared at 38.3, 44.4, 64.8 and 77.6°, corresponding to the Miller indices (1 1 1), (2 0 0), (2 2 0) and (3 1 1) planes of Au, respectively to the face-center- cubic (fcc) Au crystallographic structures (JCPDS card number 4-0784).(Shanmugam and Kim 2016) Furthermore, peaks marked with asterisks appeared at 30.4, 35.3, 50.7 and 60.4° (Figure S3) were assigned to the (1 2 1), (1 1 3), (1 4 0), and (4 2 1) planes of ITO substrate (JCPDS card number 89-4599).

Here, we present a possible formation mechanism for the $M13_{4E}$ assisted electrochemical co-deposition of Au-DNs as follows; in the first step, Au precursor $AuCl_4^-$ get attached at the $-NH_2$ groups of the glutamic acid (Figure 1) present in the 4E peptides led to an ammine chloride complex. (Manivannan and Ramaraj 2012a) In the next step, when the constant potential of −0.2 V is applied, the $AuCl_4^-$ were slowly released from the attachment sites and reduced to Au^0. In order to get stabilize, Au^0 tend to aggregate to form Au^0 nuclei, which is predicted to be hosted by $M13_{4E}$. The nucleated Au^0 will form Au atomic clusters and at the same time –COOH of the 4E peptides tend to attach at the ITO surface and became the growth centres for DNs. These $M13_{4E}$ attached Au atomic clusters acts as seeds and further reduction led to the growth of Au-DNs. Here slow release of Au^{3+} from the above mentioned ammine chloride complex is the key factor to decrease the reduction rate of non-equilibrium hence, anisotropic growth had occurred.

3.2. Electrocatalytic studies

In order to investigate the effect of Au-DNs, CVs and LSVs for different modified electrodes in the absence and presence of NO_2^- at pH 7.2 were compared in the potential range 0 – 1.2 V

(Figure 4). Figure 4A and B displays CVs recorded at the ITO/Au (a), ITO/Au_{wild} (b), ITO/Au_{Y3E} (c) and ITO/Au_{4E} (d) electrodes in 0.1 M PBS before and after adding NO_2^-, respectively. The characteristic oxidation and reductions peaks (Manivannan and Ramaraj 2012b) were noticed for all the four Au nanostructured electrodes, indicating the presence of crystalline Au NSs at the electrode surfaces (Figure 4A). As shown in Figure 4B, while introducing 1 mM of NO_2^- into the electrolyte, increase in anodic peak current (mass normalized) around 0.85 V is clearly observed, indicating that the NO_2^- is oxidized in the presence of Au NSs. As can be seen that the ITO/Au_{4E} electrode (Figure 4B(d)) showed improved catalytic response toward NO_2^- oxidation when compared to other electrodes. Furthermore, comparison among the ITO/Au_{4E} electrode (Figure 4C) fabricated at different concentrations of $M13_{4E}$ indicates that higher catalytic response is noticed when the concentration of $M13_{4E}$ was 0.005 mg/mL (Figure 4C(c)). It is well known that Au dendritic nanostructures providing the more active sites which can efficiently convert the adsorbed intermediates in to final products. Besides electrochemical stability and activity (provides more sites for adsorbing the intermediates) of the Au dendritic nanostructures also contributing increased active sites. Hence, the obtained flower-like nanostructures in the presence of excess M13 viruses (concentration higher than 0.005mg/mL), having the less catalytic activity than the dendritic nanostructures. CVs recorded at ITO/Au_{4E} electrode (fabricated in the presence of 0.005 mg/mL of $M13_{4E}$) for the absence (a) and presence (b) of 1 mM of NO_2^- is given in Figure 4D. At the surface of the Au-DNs, direct oxidation of NO_2^- produces increased anodic current with a well-defined, sharp peak at 0.85 V (Figure 4D(b)). It is well demonstrated that the use of Au-DNs could act as an effective electron transfer mediator to enhance the kinetics of the electrochemical process. Also, in the reverse scan there is no presence of any cathodic peak or increase in the peak current of Au oxide reduction peak due to NO_2^- was observed. In one hand, anodic oxidation of NO_2^- is desirable because nitrate (NO_3^-) is the ultimate product without any interference, but occurs at relatively high over potential. On the other hand, primary disadvantage of the cathodic reduction of NO_2^- is the

interferences from a few products depending on the condition of electrodes and nature of electrocatalysts.(Heinecke et al. 2013) Therefore, these results confirming that Au-DNs fabricated in the presence of $M13_{4E}$ demonstrated improved electrocatalytic activity than that of Au NSs fabricated without M13, $M13_{wild}$ and $M13_{Y3E}$. Therefore, the corresponding NO_2^- oxidation at the ITO/Au_{4E} electrode is shown as follows (eq 3):

$$NO_2^- + H_2O \rightarrow NO_3^- + 2H^+ + 2e^- \quad (3)$$

Furthermore, ECSA values were derived from the CVs recorded at the ITO/Au_{4E} electrode ($M13_{4E}$: 0.005 mg/mL), which is fabricated with different deposition time and correlated with their electrocatalytic properties toward NO_2^- (Figure S4 and Table S1). It was observed that, modified electrode fabricated at 500 s having higher ECSA value due to its well-branched dendritic NSs and thus showed higher catalytic activity toward NO_2^-. In addition, to reveal the role of 4E peptides of $M13_{4E}$, we have carried out the fabrication of ITO/Au electrode in the presence of native 4E peptides as an additive in the electrolyte. The structure and its catalytic activities were compared with the electrode prepared using $M13_{4E}$ as shown in Figure 5. From the SEM analysis (Figure 5(A–B1)), typical dendritic NSs were not observed in the presence of native 4E peptides as an additive, only flower-like NSs were obtained. This observation adds the evidence that only 4E peptides of the $M13_{4E}$ was not responsible for the dendritic NSs. 4E peptides displayed M13 synergistically offers its filamentous structure as the nucleation sites for the Au-DNs growth at the ITO/Au_{4E} electrode. Furthermore, ITO/Au_{4E} electrode showing higher ECSA, specific and mass activities toward NO_2^- (Figure 5C,D and S5). Since the native peptides are highly expensive and poor in their solubility, here they were displayed on the M13 surface by low-cost methodology and considerable efficiencies were obtained. Hence, present fabrication methodology can overcome several challenges in developing low cost and highly sensitive biosensor-probes.

3.3. Electrochemical biosensor studies

Electrochemical biosensor for NO_2^- is constructed at the ITO/Au_{4E} electrode ($M13_{4E}$: 0.005 mg/mL) and responses were studied by LSVs by injecting each 100 µM of NO_2^- and the results are summarized in Figure 6. At the sensor electrode, Au-DNs exhibited high sensitivity and stable response and the catalytic current is proportional to the concentration of analyte. A linear dependence of NO_2^- oxidation peak current was obtained with a correlation coefficient (R^2) of 0.995 and sensitivity is calculated as 0.190 µA/µM. Selectivity of the constructed biosensor is an important parameter for applying the developed materials for its practical application. Here the selectivity of proposed biosensor is investigated by detecting 100 µM NO_2^- with the addition of most possible interference species (cations, anions and biomolecules) into the PBS solution. Concentration of interfering ions and biomolecules were fixed to 4000 µM. As it can be seen in Figure S6, determination of 100 µM NO_2^- is not interfered by the presence of cations, anions and biomolecules including Ca^{2+}, Na^+, K^+, SO_4^{2-}, NO_3^-, CO_3^{2-} ascorbic acid and glucose in a 40-fold concentration, which indicates that this system owns a highly selective recognition only for NO_2^-. It is noteworthy to mention that while monitoring the individual interference (Figure S6D), NO_3^- and glucose causes current response of ITO/Au_{4E} electrode and it can be attributed to their very high concentrations (4000 µM). Besides in the presence of cations (Figure S6A) and anions (Figure S6B), considerable increase in the over potential for NO_2^- oxidation were noticed whereas such shift was not observed in the presence of biomolecules (Figure S6C). Therefore, this proposed method of applying M13 as additives for electrodepositing the Au NSs and the developed NO_2^- biosensor appears to be highly selective in the presence of tested most common interference species.

4. Conclusions

In summary, we have demonstrated the electrodeposition of Au-DNs using engineered M13 viruses as an additive and use them as a biosensor electrode for highly sensitive NO_2^- detection. Sensor electrode exhibited good selectivity toward target analyte from the most possible interferences. Here we demonstrated the importance of virus as additives for metal nucleation to

synthesize biotemplated materials. Only 4E peptides expressed M13 led to dendritic NSs whereas wild-type and Y3E peptides expressed M13 were not. Au-DNs at the $M13_{4E}$ applied electrode exhibited significantly higher electrocatalytic activity when compared to without M13 or native 4E peptides or those of $M13_{Wild}$ and $M13_{Y3E}$. The use of peptides as structure directing agents are well known and such peptides are highly expensive, here we demonstrated that peptides expressed on the virus surfaces as an additive to grow Au-DNs and it is highly cost effective. It is clearly demonstrated that due to the engineered peptides, biomolecules can provide general strategy for the growth of advanced catalysts with enhanced electrocatalytic and sensing ability. This simple biotemplating approach can be extended to other metals and metal oxides to obtain the variations in morphology and could be applied as electrode materials for sensors and energy harvesting applications.

Associated Content

Supporting Information

SEM-EDX analysis at the ITO/Au_{4E} electrode; SEM analysis of concentration dependent growth; XRD analysis; time dependent growth and its sensor studies; specific activity comparison between $M13_{4E}$ and native 4E peptide; selectivity studies; summary of ECSA values

Acknowledgements

This work was partially supported by the Incheon National University (International Cooperative) Research Grant in 2012.

References:

Avery, K.N., Schaak, J.E., Schaak, R.E., 2009. M13 Bacteriophage as a biological scaffold for magnetically-recoverable metal nanowire catalysts: Combining specific and nonspecific interactions to design multifunctional nanocomposites. Chemistry of Materials 21(11), 2176-2178.

Bharath, G., Madhu, R., Chen, S.M., Veeramani, V., Mangalaraj, D., Ponpandian, N., 2015. Solvent-free mechanochemical synthesis of graphene oxide and Fe_3O_4-reduced graphene oxide nanocomposites for sensitive detection of nitrite. Journal of Materials Chemistry A 3(30), 15529-15539.

Correia, A.N., Mascaro, L.H., Machado, S.A.S., Avaca, L.A., 1997. Active surface area determination of Pd-Si alloys by H-adsorption. Electrochimica Acta 42(3), 493-495.

Heinecke, J.L., Khin, C., Pereira, J.C.M., Suárez, S.A., Iretskii, A.V., Doctorovich, F., Ford, P.C., 2013. Nitrite reduction mediated by heme models. Routes to NO and HNO? Journal of the American Chemical Society 135(10), 4007-4017.

Hemminga, M.A., Vos, W.L., Nazarov, P.V., Koehorst, R.B.M., Wolfs, C.J.A.M., Spruijt, R.B., Stopar, D., 2010. Viruses: Incredible nanomachines. New advances with filamentous phages. European Biophysics Journal 39(4), 541-550.

Hong, W., Xu, Y., Lu, G., Li, C., Shi, G., 2008. Transparent graphene/PEDOT–PSS composite films as counter electrodes of dye-sensitized solar cells. Electrochemistry Communications 10(10), 1555-1558.

Jin, H., Won, N., Ahn, B., Kwag, J., Heo, K., Oh, J.W., Sun, Y., Cho, S.G., Lee, S.W., Kim, S., 2013. Quantum dot-engineered M13 virus layer-by-layer composite films for highly selective and sensitive turn-on TNT sensors. Chemical Communications 49(54), 6045-6047.

Khan, M.M.I., Haque, A.M.J., Kim, K., 2013. Electrochemical determination of uric acid in the presence of ascorbic acid on electrochemically reduced graphene oxide modified electrode. Journal of Electroanalytical Chemistry 700, 54-59.

Ki, T.N., Wartena, R., Yoo, P.J., Liau, F.W., Yun, J.L., Chiang, Y.M., Hammond, P.T., Belcher, A.M., 2008. Stamped microbattery electrodes based on self-assembled M13 viruses. Proceedings of the National Academy of Sciences of the United States of America 105(45), 17227-17231.

Kim, J., Rheem, Y., Yoo, B., Chong, Y., Bozhilov, K.N., Kim, D., Sadowsky, M.J., Hur, H.G., Myung, N.V., 2010. Peptide-mediated shape-and size-tunable synthesis of gold nanostructures. Acta Biomaterialia 6(7), 2681-2689.

Kim, K., Kang, I., Manivannan, S., 2016. Platinum Electrodeposition on in-Situ Grown Prussian Blue Nanostructures and Reduced Graphene Oxide Composite for Synergistic Methanol Oxidation. Meeting Abstracts MA2016-02(46), 3397-3397.

Korkmaz, N., 2013. Recombinant bacteriophages as gold binding bio-templates. Colloids and Surfaces B: Biointerfaces 112, 219-228.

Lee, S.K., Yun, D.S., Belcher, A.M., 2006. Cobalt ion mediated self-assembly of genetically engineered bacteriophage for biomimetic Co-Pt hybrid material. Biomacromolecules 7(1), 14-17.

Lee, Y.J., Lee, Y., Oh, D., Chen, T., Ceder, G., Belcher, A.M., 2010. Biologically activated noble metal alloys at the nanoscale: For lithium ion battery anodes. Nano Letters 10(7), 2433-2440.

Manivannan, S., Ramaraj, R., 2012a. Assemblies of silicate sol-gel matrix encapsulated core/shell Au/Ag nanoparticles: Interparticles surface plasmon coupling. Journal of Nanoparticle Research 14(6).

Manivannan, S., Ramaraj, R., 2012b. Synthesis of cyclodextrin-silicate sol-gel composite embedded gold nanoparticles and its electrocatalytic application. Chemical Engineering Journal 210, 195-202.

Mao, C., Flynn, C.E., Hayhurst, A., Sweeney, R., Qi, J., Georgiou, G., Iverson, B., Belcher, A.M., 2003. Viral assembly of oriented quantum dot nanowires. Proceedings of the National Academy of Sciences of the United States of America 100(12), 6946-6951.

Mateu, M.G., 2011. Virus engineering: Functionalization and stabilization. Protein Engineering, Design and Selection 24(1-2), 53-63.

Mehmeti, E., Stanković, D.M., Hajrizi, A., Kalcher, K., 2016. The use of graphene nanoribbons as efficient electrochemical sensing material for nitrite determination. Talanta 159, 34-39.

Nam, K.T., Kim, D.W., Yoo, P.J., Chiang, C.Y., Meethong, N., Hammond, P.T., Chiang, Y.M., Belcher, A.M., 2006. Virus-enabled synthesis and assembly of nanowires for lithium ion battery electrodes. Science 312(5775), 885-888.

Nam, Y.S., Park, H., Magyar, A.P., Yun, D.S., Pollom, T.S., Belcher, A.M., 2012. Virus-templated iridium oxide-gold hybrid nanowires for electrochromic application. Nanoscale 4(11), 3405-3409.

Palanisamy, S., Karuppiah, C., Chen, S.-M., Periakaruppan, P., 2014. Highly sensitive and selective amperometric nitrite sensor based on electrochemically activated graphite modified screen printed carbon electrode. Journal of Electroanalytical Chemistry 727, 34-38.

Park, J.P., Do, M., Jin, H.-E., Lee, S.-W., Lee, H., 2014. M13 Bacteriophage Displaying DOPA on Surfaces: Fabrication of Various Nanostructured Inorganic Materials without Time-Consuming Screening Processes. ACS Applied Materials & Interfaces 6(21), 18653-18660.

Peteu, S.F., Boukherroub, R., Szunerits, S., 2014. Nitro-oxidative species in vivo biosensing: Challenges and advances with focus on peroxynitrite quantification. Biosensors and Bioelectronics 58, 359-373.

Pham, X.H., Li, C.A., Han, K.N., Huynh-Nguyen, B.C., Le, T.H., Ko, E., Kim, J.H., Seong, G.H., 2014. Electrochemical detection of nitrite using urchin-like palladium nanostructures on carbon nanotube thin film electrodes. Sensors and Actuators, B: Chemical 193, 815-822.

Qi, H., Wang, F., Petrenko, V.A., Liu, A., 2014. Peptide microarray with ligands at high density based on symmetrical carrier landscape phage for detection of cellulase. Analytical Chemistry 86(12), 5844-5850.

Radhakrishnan, S., Krishnamoorthy, K., Sekar, C., Wilson, J., Kim, S.J., 2014. A highly sensitive electrochemical sensor for nitrite detection based on Fe2O3 nanoparticles decorated reduced graphene oxide nanosheets. Applied Catalysis B: Environmental 148–149, 22-28.

Rao, D., Sheng, Q., Zheng, J., 2016. Self-assembly preparation of gold nanoparticle decorated 1-pyrenemethylamine functionalized graphene oxide-carbon nanotube composites for highly sensitive detection of nitrite. Analytical Methods 8(24), 4926-4933.

Sambrook, J., Russell, D.W., 2001. Molecular Cloning: A Laboratory Manual. Cold Spring Harbor Laboratory Press.

Shanmugam, M., Kim, K., 2016. Electrodeposited gold dendrites at reduced graphene oxide as an electrocatalyst for nitrite and glucose oxidation. Journal of Electroanalytical Chemistry 776, 82-92.

Shervedani, R.K., Amini, A., Sadeghi, N., 2016. Electrografting of thionine diazonium cation onto the graphene edges and decorating with Au nano-dendrites or glucose oxidase: Characterization and electrocatalytic applications. Biosensors and Bioelectronics 77, 478-485.

Shin, I.-S., Lim, H.-C., Oh, J.-W., Lee, J.-K., Kim, T.H., Kim, H., 2011. Fast-response light-emitting electrochemical cells based on neutral iridium(III) complex. Electrochemistry Communications 13(1), 64-67.

Smith, G.P., Petrenko, V.A., 1997. Phage display. Chemical Reviews 97(2), 391-410.

Stevens, M.M., Flynn, N.T., Wang, C., Tirrell, D.A., Langer, R., 2004. Coiled-Coil Peptide-Based Assembly of Gold Nanoparticles. Advanced Materials 16(11), 915-918.

Sun, M., Ma, W., Xu, L., Wang, L., Kuang, H., Xu, C., 2014. Chirality of self-assembled metal-semiconductor nanostructures. Journal of Materials Chemistry C 2(15), 2702-2706.

Teymourian, H., Salimi, A., Khezrian, S., 2013. Fe3O4 magnetic nanoparticles/reduced graphene oxide nanosheets as a novel electrochemical and bioeletrochemical sensing platform. Biosensors and Bioelectronics 49, 1-8.

Trasatti, S., Petrii, O.A., 1992. Real surface area measurements in electrochemistry. Journal of Electroanalytical Chemistry 327(1-2), 353-376.

Wu, X., Kuang, H., Hao, C., Xing, C., Wang, L., Xu, C., 2012. Paper supported immunosensor for detection of antibiotics. Biosensors and Bioelectronics 33(1), 309-312.

Xiao, J., Qi, L., 2011. Surfactant-assisted, shape-controlled synthesis of gold nanocrystals. Nanoscale 3(4), 1383-1396.

Xu, L., Yin, H., Ma, W., Kuang, H., Wang, L., Xu, C., 2015. Ultrasensitive SERS detection of mercury based on the assembled gold nanochains. Biosensors and Bioelectronics 67, 472-476.

Yadav, D.K., Ganesan, V., Sonkar, P.K., Gupta, R., Rastogi, P.K., 2016. Electrochemical investigation of gold nanoparticles incorporated zinc based metal-organic framework for selective recognition of nitrite and nitrobenzene. Electrochimica Acta 200, 276-282.

Yue, R., Lu, Q., Zhou, Y., 2011. A novel nitrite biosensor based on single-layer graphene nanoplatelet–protein composite film. Biosensors and Bioelectronics 26(11), 4436-4441.

Zhang, C., Song, C., Fry, H.C., Rosi, N.L., 2014. Peptide conjugates for directing the morphology and assembly of 1D nanoparticle superstructures. Chemistry - A European Journal 20(4), 941-945.

Zin, M.T., Ma, H., Sarikaya, M., Jen, A.K.Y., 2005. Assembly of gold nanoparticles using genetically engineered polypeptides. Small 1(7), 698-702.

Figures

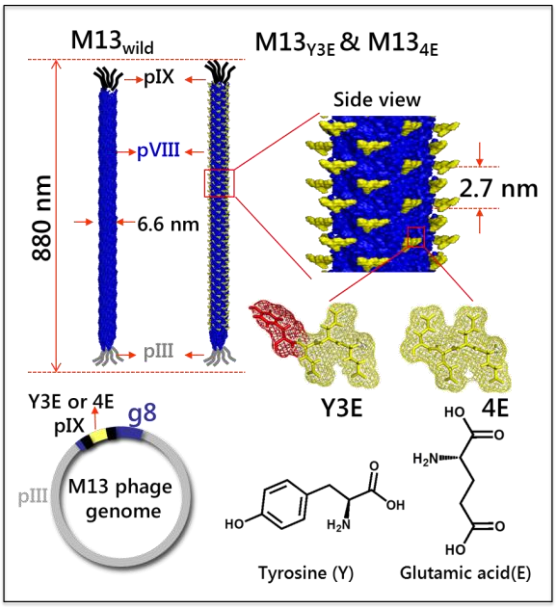

Figure 1. Schematic representation of $M13_{wild}$ and $M13_{4E}$.

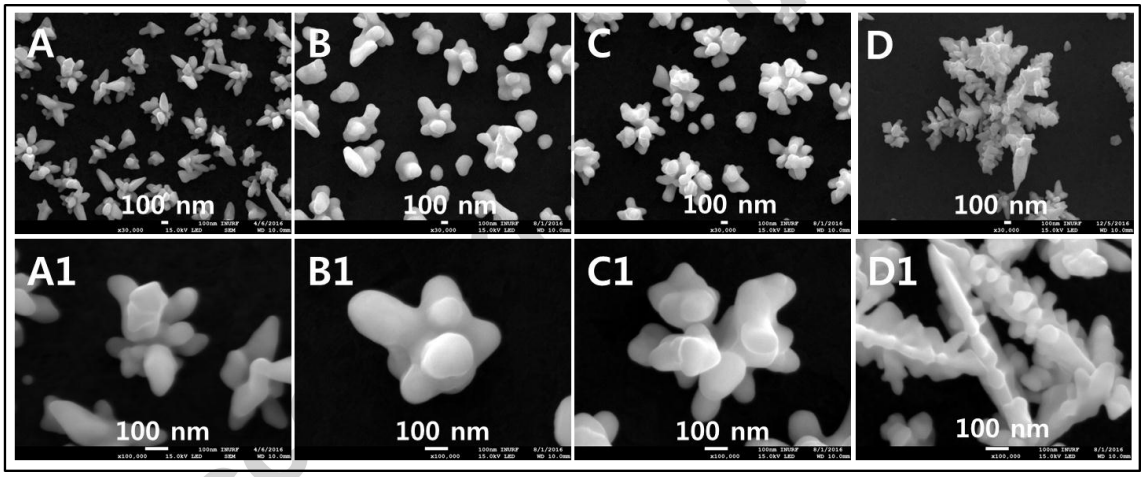

Figure 2. (**A** to **D1**) SEM images of (**A, A1**) ITO/Au, (**B, B1**) ITO/Au_{wild}, (**C, C1**) ITO/Au_{Y3E} and (**D, D1**) ITO/Au_{4E} electrodes at different magnifications.

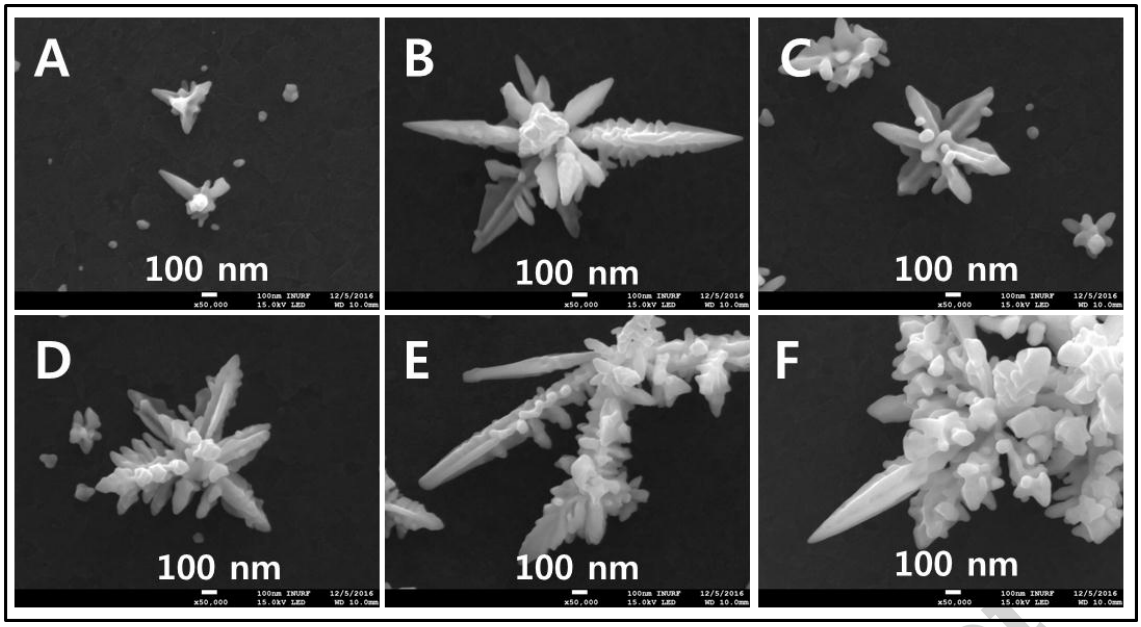

Figure 3. (**A** to **E**) SEM images of ITO/Au_{4E} electrode at different deposition time; **A**: 5 s, **B**: 10 s, **C**: 20 s, **D**: 50 s, **E**: **1**00 s and F: 500 s.

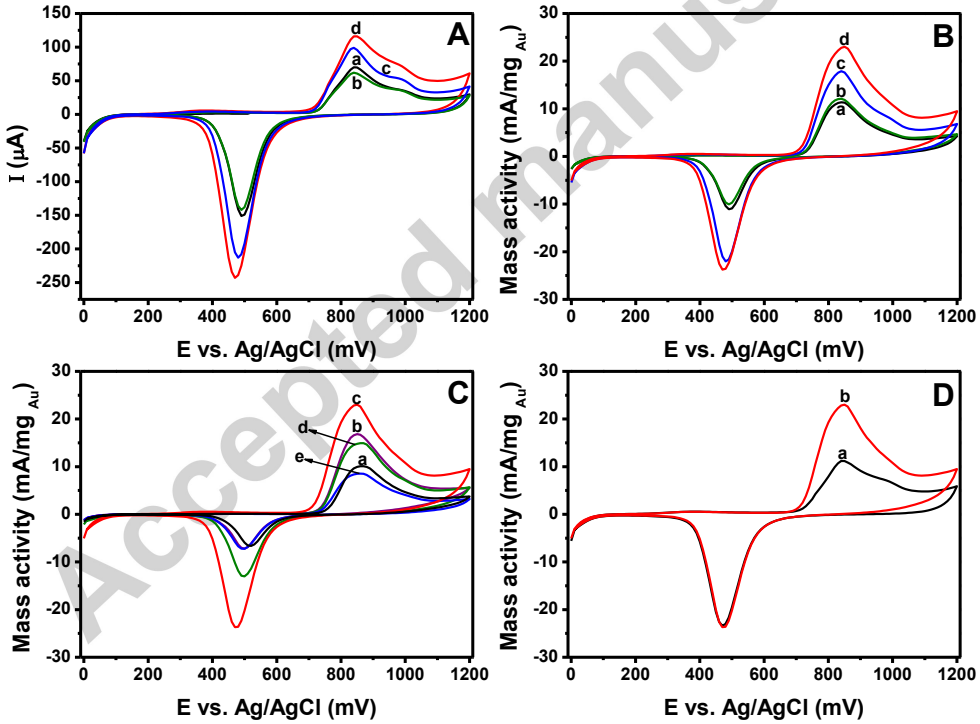

Figure 4. (**A, B**) CVs recorded at the (**a**) ITO/Au, (**b**) ITO/Au_{wild}, (**c**) ITO/Au_{Y3E} and (**d**) ITO/Au_{4E} electrodes in (**A**) 0.1 M PBS (pH: 7.2) (**B**) injected with 1 mM of NO_2^-. (**C**) CVs recorded in the presence of 1 mM of NO_2^- at the ITO/Au_{4E} electrode fabricated at different $M13_{4E}$ concentration; **a**: no $M13_{4E}$ **b**: 0.001 mg/mL, **c**: 0.005 mg/mL, **d**: 0.01 mg/mL and **e**: 0.05 mg/mL. (**D**) CVs recorded at

ITO/Au_{4E} electrode in the (a) absence and (b) presence of 1 mM of NO_2^-. All the CVs were recorded at the scan rate of 50 mVs^{-1}.

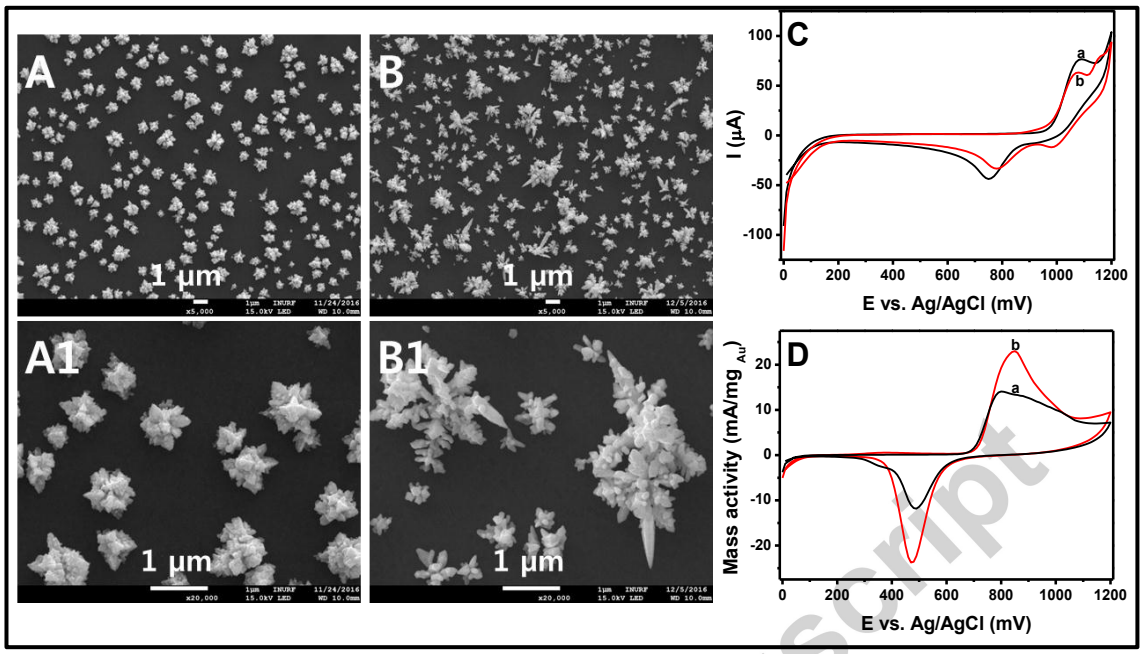

Figure 5. (**A-B1**) SEM images and (**C,D**) CVs recorded at the (A,A1 and **a**) ITO/Au-4E Pep, and (**b**) ITO/Au_{4E} electrodes in (**C**) 0.5 M H_2SO_4 and in (**D**) 0.1 M PBS (pH: 7.2) injected with 1 mM of NO_2^-. All the CVs were recorded at the scan rate of 50 mVs^{-1}.

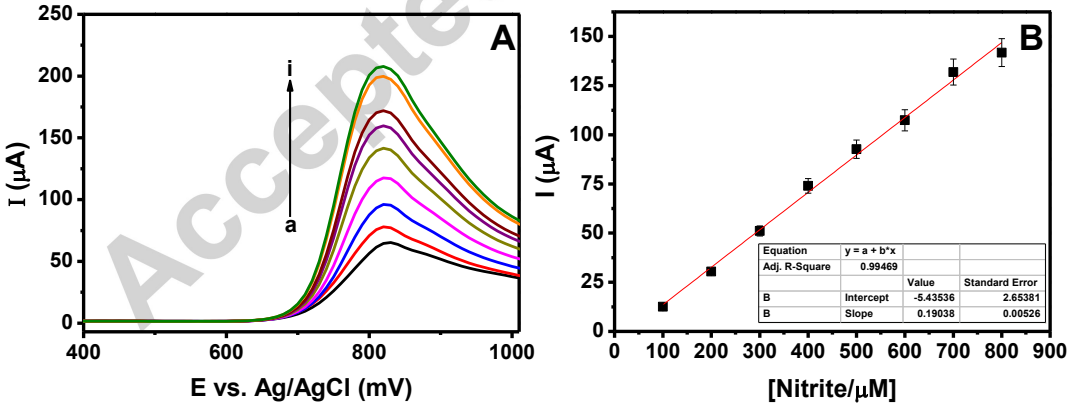

Figure 6. (**A**) LSVs recorded at the ITO/Au_{4E} electrodes in 0.1 M PBS (pH: 7. 2) for (**a**) 0 µM, (**b**) 100 µM, (**c**) 200 µM, (**d**) 300 µM, (**e**) 400 µM, (**f**) 500 µM, (**g**) 600 µM, (**h**) 700 µM and (**i**) 800 µM of NO_2^-. (**B**) Corresponding calibration plot.

Highlights:

- M13 viruses as an additive for Au electrodeposition.
- 4E peptides engineered M13 viruses led to dendritic morphology.
- Improved sensitivity and selectivity toward nitrite ions.